Ionics (2014) 20:1501–1510
DOI 10.1007/s11581-014-1241-x

REVIEW

Research status in preparation of $FePO_4$: a review

Yong-ming Zhu · Ze-wen Ruan · Shen-zhi Tang · Venkataraman Thangadurai

Received: 25 June 2014 / Revised: 27 August 2014 / Accepted: 31 August 2014 / Published online: 3 October 2014
© Springer-Verlag Berlin Heidelberg 2014

Abstract The cathode is the most important component of a lithium-ion battery. The olivine structure lithium iron phosphate ($LiFePO_4$) with its numerous appealing features, such as high theoretical capacity, acceptable operating voltage, increased safety, environmental benignity, and low cost, has attracted extensive interest as a potential cathode material for Li-ion batteries. As a precursor, $FePO_4$ can be used to produce $LiFePO_4$ on a large scale with high bulk density, discharge rate, and capacity. This can be realized by controlling the crystal size and morphology of $FePO_4$. The characteristics, structure, and synthesis methods of $FePO_4$ are discussed in this review. The relative merits of these synthetic methods, as well as some suggestions on how to improve them, are also presented.

Keywords Olivine phosphate · $FePO_4$ · $LiFePO_4$ · Li cathode · Lithium-ion battery

Introduction

In recent years, lithium-ion battery has been widely used due to its high voltage and high specific and volumetric energy densities, and easy transportability. Currently, a key factor in the lithium-ion battery is the research of high-voltage cathode materials that has mainly focused on layered transition metal oxides $LiMO_2$ (M = Co, Ni) and spinel structures LiM_2O_4 (M = Mn, Ni) [1–7]. The widely used $LiCoO_2$-based batteries have problems regarding safety, cost, and environment, which are difficult to overcome. Searching for cheaper, more secure, stable and environmentally friendly cathode materials has become a top priority. $LiNiO_2$, which has a similar structure as $LiCoO_2$, has an advantage with respect to cost and raw materials. However, the difficulties in the synthetic process, the unstable structure, and the poor chemical stability become shortcomings of $LiNiO_2$ to limit its application. Finally, the spinel $LiMnO_4$ has advantages in rich resources of raw materials, low cost, increased safety, environmental friendliness, and simple synthetic process. But further research, development, and application of the synthetic process are hindered by the Jahn–Teller effect in the process of charging and discharging.

In 1997, the Goodenough group [8] first reported that olivine structure lithium iron phosphate ($LiFePO_4$) can display the intercalation/de-intercalation of lithium ions reversibly. Since, $LiFePO_4$ has been considered to be the most promising cathode material for the lithium-ion battery due to its nontoxicity, low cost, and high thermal stability characteristics [9–17]. Unlike other Li electrodes, $LiFePO_4$ exhibits almost theoretical capacity of about 170 mAh g^{-1} [2], and $Li_4Ti_5O_{12}$ also almost shows theoretical capacity (Fig. 1); however, it must be mentioned that the practical capacity depends on C-rate.

The iron sources for preparation of lithium iron phosphate can be divided into trivalent iron sources [18–24] and divalent iron sources [25, 26]. Divalent iron sources are expensive and easily oxidized. Even in an inert atmosphere, it is still difficult to avoid the appearance of Fe^{3+} impurity. $FePO_4$, as a trivalent iron source, which has a low cost and a high chemical stability, is an ideal material for the synthesis of lithium iron phosphate. $LiFePO_4$ particles can be obtained by controlling the size and morphology of $FePO_4$ with similar characteristics, so as to achieve the target of high bulk density, high discharge rate, and high specific capacity, overcoming the limitation in

Y.-m. Zhu (✉) · Z.-w. Ruan · S.-z. Tang
Department of Applied Chemistry, Harbin Institute of Technology at Weihai, Weihai 264209, China
e-mail: kielming@hotmail.com

Y.-m. Zhu
e-mail: vthangad@ucalgary.ca

V. Thangadurai
Department of Chemistry, University of Calgary, 2500 University Drive NW, Calgary, AB T2N 1N4, Canada

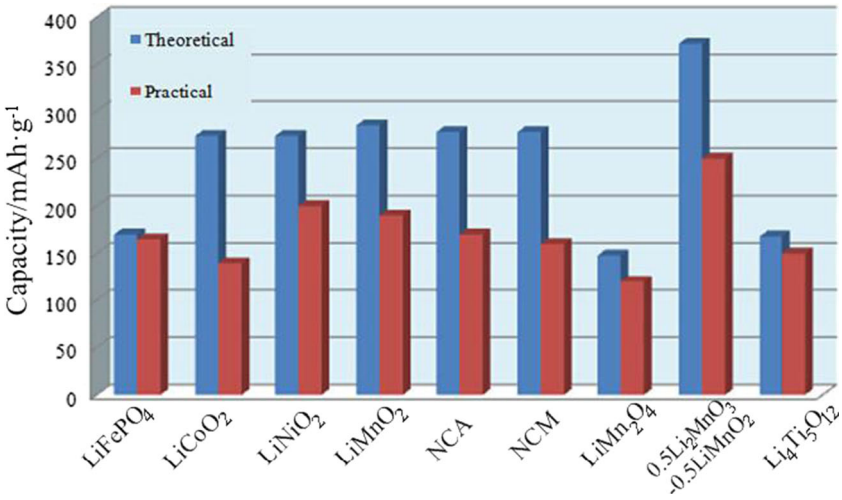

Fig. 1 A range of lithium-ion battery electrode available or currently under development and comparison of their theoretical capacity and practical capacity (NCA: $LiNi_{0.8}Co_{0.15}Al_{0.05}O_2$, NCM: $LiNi_{1/3}Co_{1/3}Mn_{1/3}O_2$)

ionic conductivity of $LiFePO_4$ to a certain extent. In this paper, we review the crystal structure, physical and chemical properties, and charging/discharging mechanism of Li iron phosphate and focus on the aspect of synthesizing iron phosphate as a precursor for lithium-ion batteries.

Crystal structure, and charging/discharging mechanism of iron phosphate

$FePO_4$ [27–30] with amorphous and different crystalline phases has already been synthesized, including heterosite, α-quartz phase, monoclinic system, and orthorhombic system. In this paper, the amorphous state and various crystalline phases of iron phosphate are discussed. However, discussion is limited to phosphate ions in the form of independent PO_4^{3-}, with no expansion to the aggregate state, meaning that the n in $(P_nO_{3n+1})^{(n+2)-}$ can only take the value 1, but not 2 or 3. Pressure and temperature can affect the structure of $FePO_4$. At normal pressure, $FePO_4$ exists as α-quartz phase, the same structure as $AlPO_4$. Each phosphorus atom and iron atom are connected to four oxygen atoms. Under a higher pressure, it changes to a tetragonal system similar to $CrPO_4$ with the cell parameters a=5.227 Å, b=7.770 Å, and c=6.332 Å. Then, under a pressure of 2.5 GPa, $FePO_4$ changes to a structure between $VCrO_4$ phase and amorphous state. Recent experimental observations suggest that $LiFePO_4/FePO_4$ interfaces are the juxtapositions of the two end members ($FePO_4$ and $LiFePO_4$) instead of solid solutions [31]. However, a solid solution might exist under particular conditions, e.g., at high temperatures [32] or in nanosized particles [33]. $FePO_4$ changes into a trigonal system at 650 °C. When the temperature rises to 705 °C, an α–β phase transition from a *P6222* to a *P31121* space group occurs [34]. Compared to the tetragonal system of $LiFePO_4$, FeO_6 octahedron is replaced by FeO_4 tetrahedron in the trigonal system [35] (Fig. 2).

The intercalation/de-intercalation process of lithium ions between $FePO_4$ and $LiFePO_4$ can be expressed as $LiFePO_4 \Leftrightarrow xFePO_4+(1-x)LiFePO_4+xLi^++xe^-$ (at 3.45 V/Li) over a large composition range, with a theoretical capacity of 170 mAh g^{-1}. To further study the intercalation process of lithium ions, Padhi et al. [8] proposed a radial model (Fig. 3a). It was suggested that this process is carried out through a two-phase interface with $FePO_4$ and $LiFePO_4$ looking like a coaxial core–shell. During charging, along with lithium-ion inserting, the interface migrates to the particle center and the interfacial area decreases, and when a critical value of area is reached, lithium-ion migration through the interface cannot support the current, and the electrochemical behavior becomes limited by the rate of diffusion (Fig. 3).

Anderson and Thomas [36] proposed a different "Mosaic model." It is believed that the de-intercalation process of lithium ions can occur over the entire surface area rather than only at the two-phase interface. With the $FePO_4$ phase of the de-lithiation region increasing gradually, the $LiFePO_4$ that remained un-reacted is coated by $FePO_4$ layers in the process, becoming a source of capacity loss. Chen et al. [37] proposed that the $FePO_4$ region and the $LiFePO_4$ region are separated by a dislocation line along the c-axis with anisotropy. In the de-intercalation process of lithium ions, the two-phase interface located at the b–c plane advances along the a-axis horizontally (for details, see Fig. 3b). Laffont et al. [31] proposed that in both the intercalation and de-intercalation processes of lithium ions, the $FePO_4$ region is always in the center of the plane, while the $LiFePO_4$ region can be found close to the edge of area (Fig. 3c). Li-ion migration paths in a unit cell of $LiFePO_4$ are represented in Fig. 4, as summarized by the above three models.

The $FePO_4$ obtained from $LiFePO_4$ with a de-intercalation process of lithium ions, referred to as heterosite structure, belongs to the same *Pnma* space group with $LiFePO_4$ with a similar structure, exhibiting a small contraction in a and b

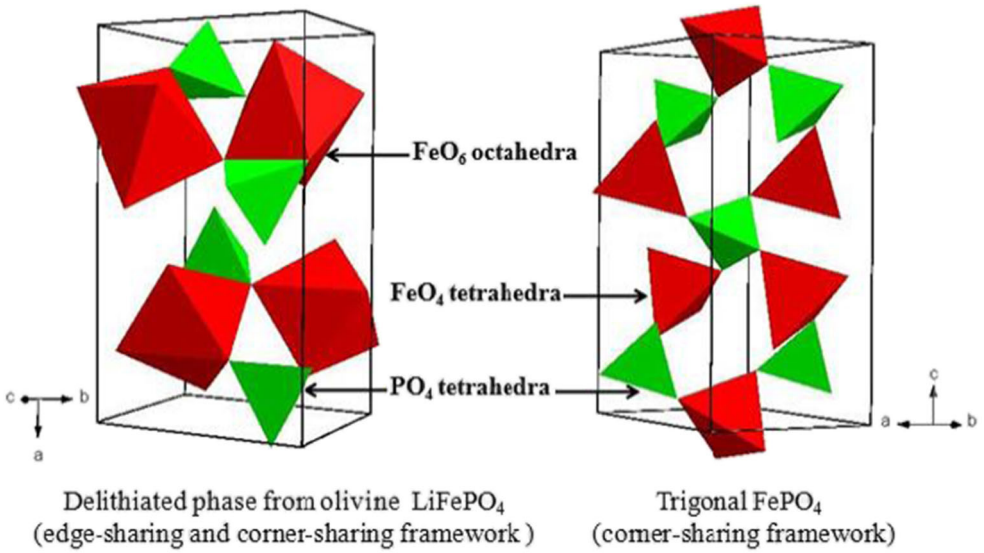

Fig. 2 Idealized crystal structures of orthorhombic and trigonal $FePO_4$

parameters and a small increase in the *c* parameter [40] (Table 1).

Synthesis of $FePO_4$ by wet chemical methods

When the synthetic process involves water or is carried out in aqueous solution, the $FePO_4$ obtained often contains crystal water, namely, $FePO_4{\cdot}xH_2O$. Figure 5 shows the thermogravimetry–differential scanning calorimetry (TG-DSC) diagram of $FePO_4{\cdot}xH_2O$ obtained by Qian et al. [41]. In the range of 18–500 °C, an obvious endothermic peak in the DSC curve and a well-defined weight loss in the TG curve were observed, corresponding to the loss of crystal water of the precursor. According to the weight loss in this process, the *x* in $FePO_4{\cdot}xH_2O$ can be estimated. The exothermic peaks at 614.46 and 690.63 °C without obvious weight loss can be assigned to structural transformation from amorphous to hexagonal $FePO_4$ and the α–β transition, respectively. Of course, TG-DSC curves vary with different synthetic methods [41, 42] but are generally similar with the previous example.

Xu et al. [40] proposed that $Fe_2P_2O_7$ appeared at 380 °C and transformed to $FePO_4$ at 460 °C during the heating process. Zhang et al. [43] divided the dehydration process of $FePO_4{\cdot}4H_2O$ into a multistep reaction by an iso-conversional rate method and analyzed it by a multivariate nonlinear regression method. They concluded that no branching reaction existed, and the most probable model for the dehydration process is a two-step consecutive reaction with kinetic parameters, such as activation energy and pre-exponential calculated out, for each of the two steps. The most probable kinetic model was estimated with a multivariate nonlinear regression method assuming a two-step consecutive reaction: D4→Fn. The activation energy *E* and $\ln(A/s^{-1})$ of D4 were 79.62 kJ mol^{-1} and 19.35. Those of Fn were 103.04 kJ mol^{-1} and 25.38 [43].

Boonchom and Danvirutai [44] studied the thermal decomposition kinetics of $FePO_4{\cdot}3H_2O$ in air. The $FePO_4{\cdot}3H_2O$ decomposed in two steps after 50 °C: the first and second decomposition steps are the loss of one and two molecules of water in crystallization, respectively. The results indicated that

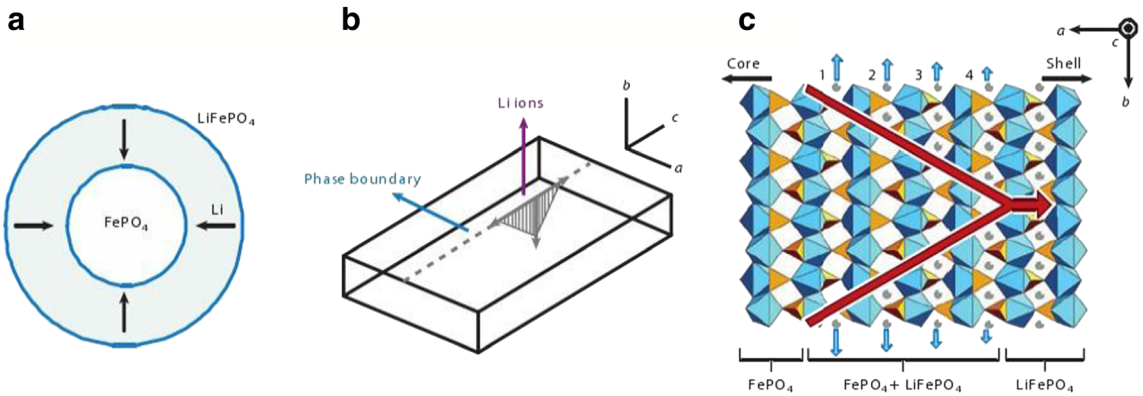

Fig. 3 Schematics of three growth models for the $LiFePO_4$–$FePO_4$ phase transition. **a** Isotropic shrinking core model, **b** anisotropic growth mode, and **c** anisotropic growth model. Reprinted from Ming et al. [38] copyright (2010), with permission from Annual Reviews

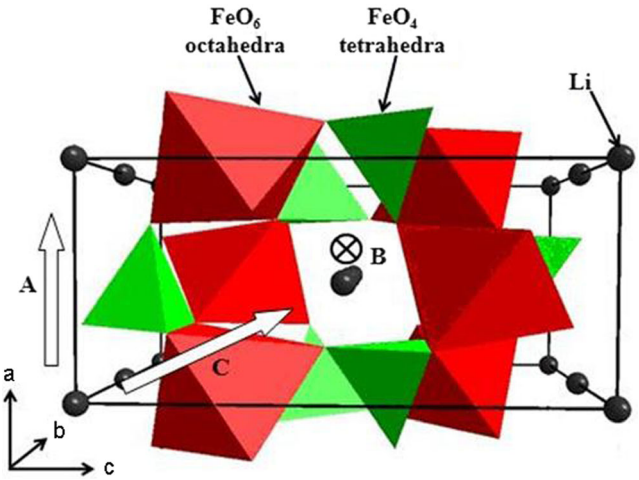

Fig. 4 Li-ion migration paths in a unit cell of $LiFePO_4$ [39]. *Mechanism A*, [010] direction; *mechanism B*, [001] direction; *mechanism C*, [101] direction. Redrawn from Saiful et al. [39] copyright (2005), with permission from the American Chemical Society

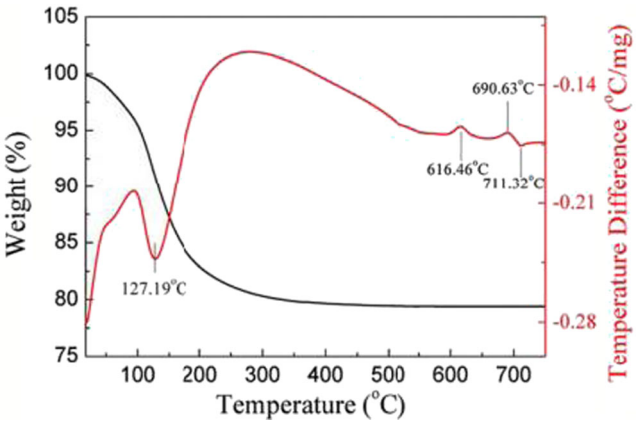

Fig. 5 TG-DSC curves of the amorphous $FePO_4$. Reprinted from Qian et al. [41] copyright (2012), with permission from Elsevier

the kinetic model, which better describes the second reaction of dehydration for $FePO_4 \cdot 3H_2O$, was the Fn model as a simple *n*th-order reaction (n=2.50). The calculated kinetic parameters of the Coats–Redfern method were E_a=77.95± 1.18 kJ mol^{-1} and ln(A/s^{-1})=14.26±0.87. Additionally, Boonchom and Puttawong [45] also reported the dehydration reaction of $FePO_4 \cdot 2H_2O$ in dynamical air atmosphere. $FePO_4 \cdot 2H_2O$ decomposed in one step, and the possible conversion function was based on the three-dimensional diffusion mechanism (D4 model), with the correlated kinetic parameters E_a=65.94±2.83 kJ mol^{-1} and ln(A/s^{-1})=8.32±1.14.

Okawa et al. [46] reported that amorphous $FePO_4$ can be obtained at 350 °C and transformed into a crystalline state at 700 °C, with the specific capacity dropped down to less than a half of the former. This can be attributed to the low activity for $FePO_4$ of the trigonal system and the formation of a glassy phase, $Fe_3P_5O_7$, covering the surface of $FePO_4$ at 580 °C. This is consistent with the study by Prosini et al. [47]. Chang et al. [48] proposed that a hexagonal layered structure of $FePO_4$ is beneficial to the diffusion of lithium ions to the center of grains, the formation of olivine $LiFePO_4$ along the *c*-axis, and the carbon coating in the reduction process, as well as the metal ion doping.

Table 1 Lattice parameters of $LiFePO_4$ and $FePO_4$ [8]

Parameters	$LiFePO_4$	$FePO_4$
Space group	*Pnma*	*Pnma*
a/Å	10.3290	9.8142
b/Å	6.0065	5.7893
c/Å	4.6908	4.7820
V/Å^3	291.02	271.70

Synthetic methods of iron phosphate

$FePO_4$ is not only used as a precursor for $LiFePO_4$, but can also be used as the cathode material directly, however, with a poor cycle performance. In addition, $FePO_4$ has also been used widely as absorbents, catalysts, antirust pigments, and additives. In the electrochemical field, it is imperative that $FePO_4$ contains no undesirable impurities. Wang et al. [49] proposed that the residual moisture in $FePO_4$ can react with Li^+ to produce LiOH (Fig. 6a, b), resulting in a higher first capacity and an irreversible degradation in the subsequent cycles. Song et al. [50] proposed that a lower activity for $FePO_4$ sintered at a temperature of 700 °C was caused by a glass phase on the surface (Fig. 6c). Secondly, it requires a high specific surface area and a high bulk density. This can be achieved by producing particles with a small size, a uniform distribution, or a spherical morphology. The electrochemical performance of $LiFePO_4$ is the most important outcome of the synthetic method. Finally, we hope that the synthetic method is simple, convenient, feasible, low cost, fast, environmentally friendly, and easy to achieve industrialization. At present, the synthetic methods of iron phosphate mainly include coordinate precipitation, sonochemical methods, hydrothermal methods, sol–gel methods, homogeneous precipitation, fluoride system methods, surfactant templates, and biologic templates.

Co-precipitation method

The co-precipitation method, also known as liquid phase precipitation method, has a comparable convenient procedure, consumes little energy, requires simple equipment, and can produce particles with small size and uniform distribution. However, this method requires similar precipitation conditions for the raw materials, which may restrict the range of choice for the starting materials. Over the past few years, there

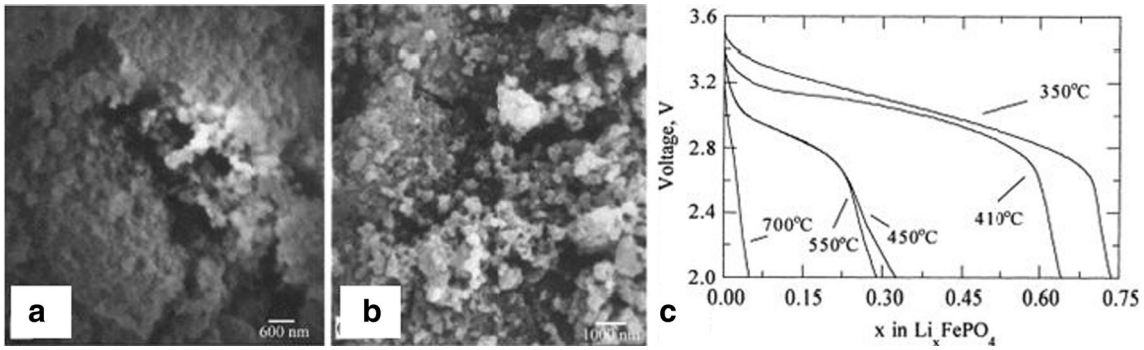

Fig. 6 SEM images of the **a** amorphous $FePO_4{\cdot}2H_2O$, **b** crystalline $FePO_4$, and **c** discharge curves of amorphous $FePO_4$ obtained at different temperatures. Reprinted from Wang et al. and Song et al. [49, 50], copyright (2012 and 2002), with permission from Elsevier

have been a number of reports regarding this method. The co-precipitation method can be done via two approaches: the liquid phase oxidation precipitation method and liquid phase non-oxidation precipitation method. The former uses divalent iron source and H_2O_2 as the oxidant, while the latter uses trivalent iron source, which is cost effective.

Generally, a stoichiometric Fe/P ratio of 1 is used. However, Hu et al. [51] believed that the electrochemical performance can be improved by increasing the H_3PO_4 proportion. $FeSO_4$ was mainly selected as the iron source for the liquid phase oxidation precipitation method, while $Fe(NO_3)_3$ and $Fe_2(SO_4)_3$ were chosen to be the iron sources for the liquid phase non-oxidation precipitation method. Chang et al. [48] used several kinds of trivalent iron sources and reached the conclusion that a maximum bulk density can be gained by using $Fe(NO_3)_3$, which was about double of the bulk density, when $Fe_2(SO_4)_3$ and $FeCl_3$ were used. H_3PO_4 or $(NH_4)_2HPO_4$ is mainly chosen as a phosphorus source. Jiang et al. [52] proposed that a $H_3PO_4/(NH_4)_2HPO_4$ ratios of 3:1 can reduce the difficulty of adjusting the pH value.

A too large concentration will result in a large number of lattice defects, while a too low concentration will lead to coarse grain. In addition, the concentration of solution can affect the amount of crystal water, meaning that a higher concentration causes a smaller value for x in $FePO_4{\cdot}xH_2O$. Both the adjustment and the final value of pH value in the synthesis are of great importance. When pH >2.2, a red-brown precipitate of $Fe(OH)_3$ appears, while a too low pH value will result in a incomplete precipitation of Fe^{3+} and waste. Ma et al. [53] proposed that a low temperature (70 °C or less) was not favorable for the $Fe(OH)_3$ to $FePO_4{\cdot}xH_2O$ conversion, while a high temperature was promoting the crystallization of $FePO_4{\cdot}xH_2O$. The whole synthesis process also needed stirring. When the stirring speed increased, the raw materials would react entirely. However, a too high speed can cause a whirlpool in the liquid center, causing uneven mixing away from the center. The $FePO_4{\cdot}xH_2O$ amorphous precipitation was collected by filtration, washed with distilled water, dried, grinded, and heated. Chang et al. [48] proposed that the aggregation of $FePO_4$ can be reduced by drying two times (drying under vapor after natural drying), and the bulk density of $FePO_4$ can be increased by nearly 50 % to 2.14 g cm^{-3} simultaneously. Xia et al. [54] reported that a small amount of Fe_2P with a good dispersion after calcination at 800 °C.

In addition, when the flow rate was controlled strictly by a constant flow pump [48], a metering pump [55], or a peristaltic pump [56], the solution was added uniformly rather than mixed directly, and a high-density $FePO_4$ was obtained. Cao et al. [56] reported that the $FePO_4$ particles of large size can get an excellent bulk density (2.03 g cm^{-3}), and the $FePO_4$ particles of middle size delivered a capacity density of 230.4 mAh cm^{-3} at a rate of 0.1C due to the relatively high bulk density and a lower electrochemical polarization. Zhu et al. [57] reported a facile co-precipitation route through which amorphous iron phosphate particles were synthesized,

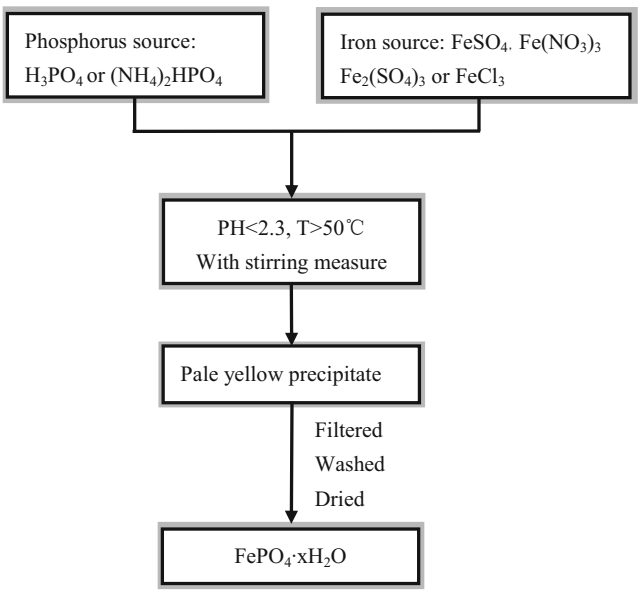

Fig. 7 Synthetic process of coordinate precipitation method [46, 48, 51–54, 56, 57]

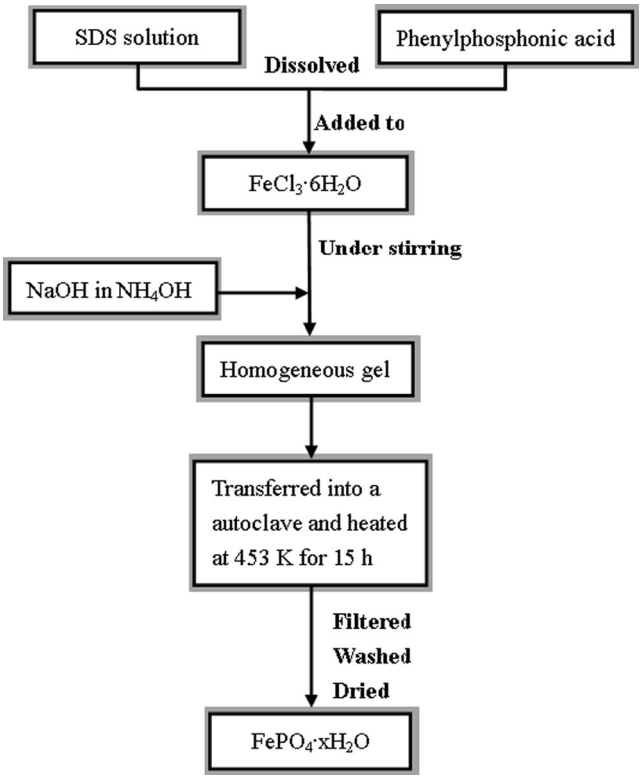

Fig. 8 Synthetic process of hydrothermal method [59]

and the $FePO_4$ obtained featured narrow size distribution, abundant porous structure, and large specific surface.

The homogeneous precipitation method, in which a precipitant is added to achieve a uniform precipitation, can be classified in the liquid phase precipitation method. Carbamide is a commonly used precipitant. Gong et al. [58] reported that the wafer-like $FePO_4$ of hexagonal structure with uniform particle size was obtained by adding a carbamide precipitant and a shape control agent. In the sonochemical method, proposed by Okawa et al. [46], an ultrasonic vibration measure was employed to initiate a series of reactions, mainly generating H_2 and H_2O_2, and achieving oxidation of $FeSO_4$. Although a different name was used, in essence, it was still in the range of the co-precipitation method. This method had the following advantages: no use of oxidation agents, reduction in reaction time, and the ability to control particle size. However, we believe that it may not be suitable for large-scale industrialization due to repeated filtration and washing. The common synthetic process is shown in Fig. 7.

Hydrothermal method

Mal et al. [59] reported that a novel organic–inorganic mesoporous $FePO_4$ had been synthesized by using sodium dodecyl sulfate (SDS) molecules as surfactant, adding $FeCl_3$ and $C_6H_5PO(OH)_2$ as raw materials under stirring, followed by a heat treatment at 453 K for 15 h in a Teflon-lined stainless steel autoclave (Fig. 8). The hydrothermal method had the following advantages: small size and uniform distribution of particles obtained, simple reaction condition, and completeness of grain growth. The use of autoclave meant that raw materials should be added all at once, that the process was extremely difficult to observe and control, and that industrial production was limited due to the small autoclave container size.

Sol–gel method

Guo [60] reported that the trigonal $FePO_4$ with a particle size of 100 nm was synthesized by using citric acid as ligand after adjusting the pH value and the ligand molar ratio. Lu et al. [61] reported that $FePO_4$ with uniform distribution was synthesized by thermal decomposition of $FeOPO(OC_6H_4COOH)_2 \cdot 0.5H_2O$ precursor prepared from a $HOPO(OC_6H_4COOH)_2$ ligand dissolved in distilled water (70 %) and ethanol (30 %) with the addition of $Fe(NO_3)_3$ drop-wise under continuous stirring (Fig. 9). It was suggested that the existence of a little residual carbon after thermal decomposition can improve the conductivity of the cathode material. The advantages of the sol–gel method were low

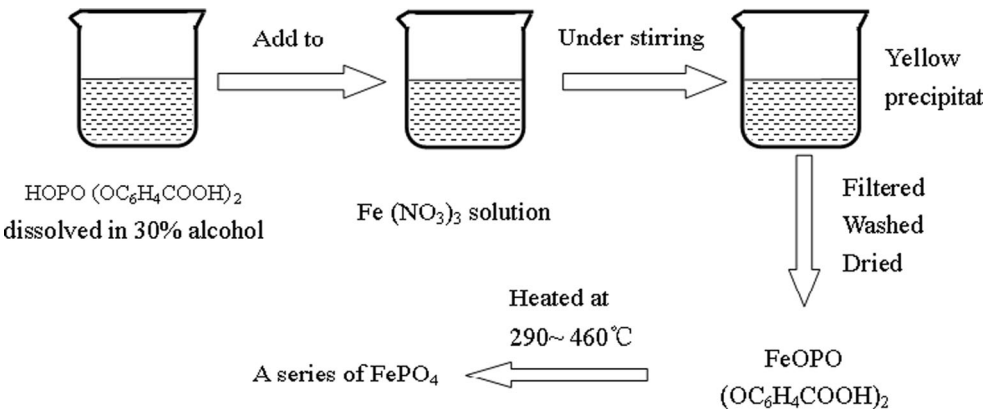

Fig. 9 Synthetic process of sol–gel method [61]

temperature and high uniformity. But a large number of micropores in the gel may cause contraction during the drying process. The best discharge capacity of the synthesized samples around 380 °C was 146 mAh g^{-1}.

Fluoride system method

Guo [60] reported that the hexagonal mesoporous $FePO_4$ with a particle size of 2.6 nm was synthesized by adding HF as mineralizer and sodium dodecyl sulfate as surfactant into $FePO_4$ (prepared by mixing Na_2HPO_4 with $Fe(NO_3)_3$ suspension and reacting at 60 °C for 2.5 h) (Fig. 10). However, the removal of impurities was cumbersome. It was proposed that neither NaF nor NH_4F can work well, while HF with a low dissociation degree could form a hydrogen bonding between $[FeHPO_4]^+$–F^- ion pairs. Also, the F^- anions had an effect on the electrostatic interaction between ion pairs and anionic surfactant micelles. They also enhanced the formation of the hexagonal mesostructured phase.

Surfactant template method

In this method, mesoporous materials are synthesized under the guide function of templates. Zhu et al. [62] reported that highly ordered hexagonal mesoporous $FePO_4$ was synthesized by adding cetyltrimethylammonium chloride (CTMACl) into $Fe_2(SO_4)_3$ and H_3PO_4 raw materials. However, it was pointed out that only 50 % of CTMACl can be removed effectively. Similarly, Shi et al. [63] took a surfactant (EO_{20}–PO_{20}–EO_{20}, Plurinic P123) as the template. They proposed that a little residual carbon would be left in $FePO_4$ after heating and a collapse of the mesoporous structure would happen in the temperature range of 500–600 °C. The mesoporous $FePO_4$ delivered enhanced specific capacity of 160 mAh g^{-1} at the first discharge process and 135 mAh g^{-1} in the following cycles at 0.1C rate. Wang et al. [64] reported that cetyltrimethylammonium bromide (CTAB) was

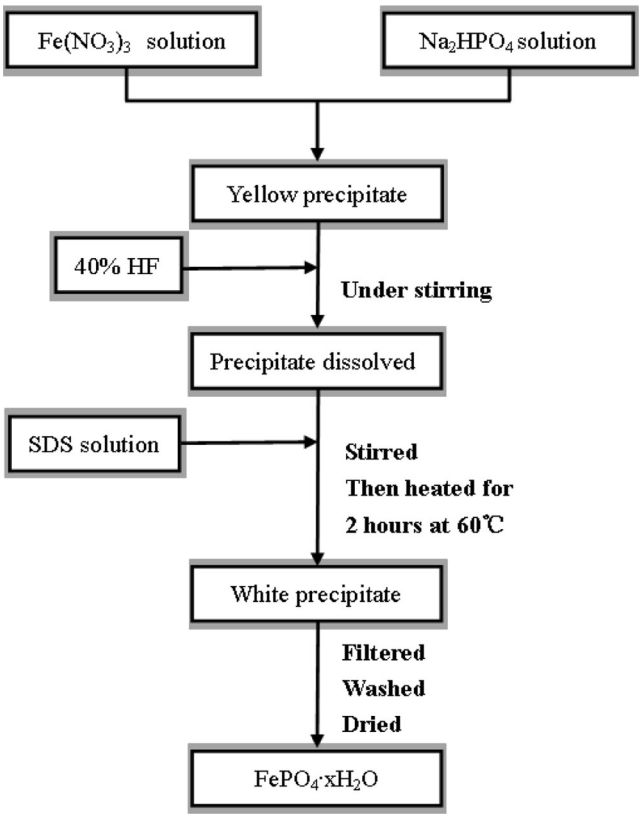

Fig. 10 Synthetic process of fluoride system method [60]

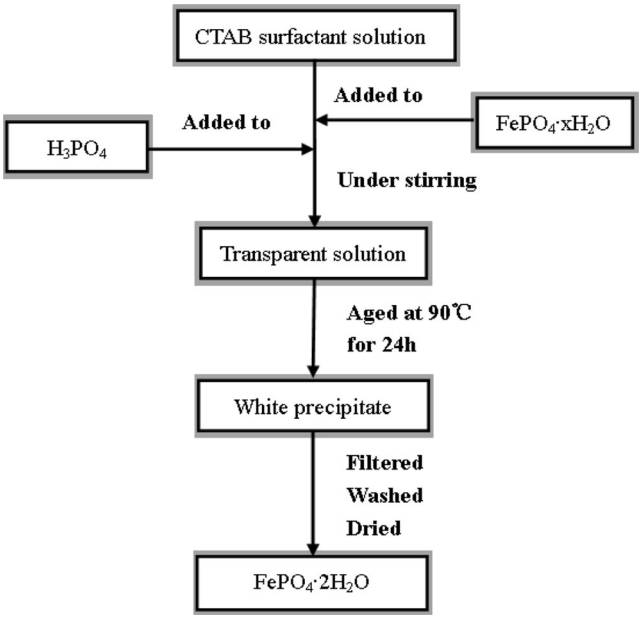

Fig. 11 Synthetic process of surfactant template method [64]

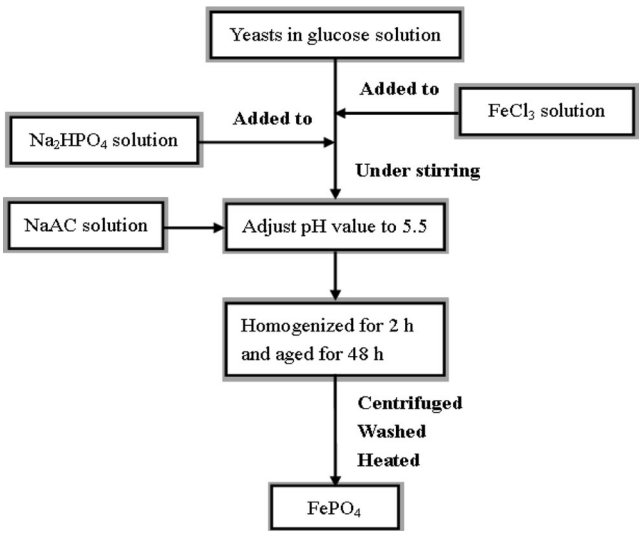

Fig. 12 Synthetic process of biologic template method [66]

also suitable to be a template (Fig. 11). The $LiFePO_4$/C nanoparticles lithiated from the obtained $FePO_4 \cdot 2H_2O$ nanoplates delivered discharge capacities of more than 150, 120, 110, 100, and 75 mAh g^{-1} at rates of 5C, 10C, 15C, 20C, and 30C, respectively.

Biologic template method

In the so-called biologic template method, organisms provided nucleation sites to regulate the grain growth. Zhou et al. [65] reported that iron phosphate nanopowders with flake morphology had been synthesized with yeast cells as a biologic template. In the synthetic process, the biologic template adsorbed Fe^{3+} cations firstly, which led to the formation of $FePO_4$. They pointed that the organisms could be removed completely after heating at 500 °C and only little conductive carbon was left. Similarly, Cao and Li [66] reported that iron phosphate hollow microspheres were obtained with pollen grains as biologic template (Fig. 12).

Other synthetic methods

Chen et al. [67] reported that crystalline $FePO_4$ had been synthesized through a reaction between iron powder, H_3PO_4, and $NH_4H_2PO_4$ in aqueous solution and mixed with conductive agent after grinding. This synthetic method was simple and low cost; however, the electrochemical performance was poor. Wu et al. [68] prepared nano $FePO_4 \cdot xH_2O$ powders by controlled crystallization method, using Fe(III) compound as the iron source. Then, the olivine nano $LiFePO_4$/C composites were obtained through carbothermal reduction process at different temperatures. The results show that the nano $LiFePO_4$/C composite calcined at 700 °C for 10 h has fine particle sizes of about 40–100 nm. The nano $LiFePO_4$/C composite cathode material can deliver an initial discharge capacity of 156.5, 134.9, 105.8, 90.3, and 80.9 mAh g^{-1} in the voltage range of 2.5–4.2 V, at a rate of 0.1C, 1C, 5C, 10C, and 15C, respectively, which exhibits good rate performance.

Okada et al. [35] reported that an increase of more than 35 % in specific capacity can be obtained by mixing P_2O_5 with Fe, ball milling with water for 24 h, and subsequent heating and ball milling without water for 24 h. Delacourt et al. [69] reported that several different hydrated iron phosphates were prepared under refluxing conditions. The low temperature solid phase method [70] took high energy consumption in the synthesis process, and the uniformity of particle size distribution was relatively poor. Qian et al. [41] reported that amorphous $FePO_4$ had been synthesized by an electrochemical synthetic method with H_3PO_4 as the electrolyte, iron as the anode, and H_2O_2 as the oxidant. This method may be a new direction to prepare $FePO_4$.

Conclusion and prospection

In this paper, the structure, properties, and various synthetic methods of iron phosphate were discussed, with a focus on the synthetic methods. One common issue that needs to be addressed is that although some researchers had synthesized $FePO_4$ of a large surface area or small particle size, the electrochemical performances of the ultimate product $LiFePO_4$ were still unknown. On one hand, to obtain an appropriate $FePO_4$ precursor, researchers should continue to increase bulk density, reduce cost, and optimize details to adapt to industrialization. On the other hand, the coordination between synthetic methods for $FePO_4$ precursor and the subsequent lithium insertion operation should be taken into consideration. In general, the method to prepare $LiFePO_4$ was mixing the $FePO_4$ precursor with a carbon source and a lithium source in a tube furnace by carbothermal reduction method, which inevitably led to a reduction of bulk density and an enlargement of particle size. At present, some researchers also take a rheological phase method [71] as well as other methods.

Acknowledgments The financial support of China Postdoctoral Science Foundation (2012M520717) and Natural Scientific Research Innovation Foundation in Harbin Institute of Technology (HIT.NSRIF.2011099) is gratefully acknowledged.

References

1. Xiong LL, Xu YL, Tao T et al (2012) Synthesis and electrochemical characterization of multi-cations doped spinel $LiMn_2O_4$ used for lithium ion batteries. J Power Sources 199:214–219
2. Fergus JW (2010) Recent developments in cathode materials for lithium ion batteries. J Power Sources 195(4):939–954
3. Seung SH, Chang GC, Kyu-Sung P (2011) Stabilizing $LiCoO_2$ electrode with an overlayer of $LiNi_{0.5}Mn_{1.5}O_4$ by using a Gravure printing method. Electrochem Commun 13(3):279–283
4. Arumugam D, Kalaignan GP (2011) Electrochemical characterizations of surface modified $LiMn_2O_4$ cathode materials for high temperature lithium battery applications. Thin Solid Films 520:338–343
5. Grigorova E, Mandzhukova TS, Khristov M et al (2011) Soft mechanochemically assisted synthesis of nano-sized $LiCoO_2$ with a layered structure. J Mater Sci 46:7106–7113
6. Zhao CH, Kang WP, Zhao SQ et al (2011) Hydrazine–hydrothermal synthesis of pure-phase O-$LiMnO_2$ for lithium-ion battery application. Micro Nano Lett 6(10):820–822
7. Shan YX, Wang QC, Meng QZ (2010) Research progress on lithium iron phosphate as lithium ion battery cathode material. Sci Technol Chem Ind 18(3):80–82
8. Padhi AK, Nanjundaswamy KS, Goodenough JB (1997) Phospho-olivines as positive-electrode materials for rechargable lithium batteries. J Electrochem Soc 144:1188–1190
9. Zhang W-J (2011) Structure and performance of $LiFePO_4$ cathode materials: a review. J Power Sources 196:2962–2970
10. Zhao Z-w, Si X-f, Liang X-x et al (2013) Electrochemical behavior of Li^+, Mg^{2+}, Na^+ and K^+ in $LiFePO_4/FePO_4$ structures. Trans Nonferrous Metals Soc China 23:1157–1164

11. Zhang Y, Huo Q-y, Du P-p et al (2012) Advances in new cathode material $LiFePO_4$ for lithium-ion batteries. Synth Met 162:1315–1326
12. Purwadi A, Dozeno J, Heryana N (2013) Testing performance of 10 kW BLDC motor and $LiFePO_4$ battery on ITB-1 electric car prototype. Procedia Technol 11:1074–1082
13. Yoon M-S, Islam M, Ur S-C (2013) The role of impurities on electrochemical properties of $LiFePO_4$ cathode material. Ceram Int 39:S647–S651
14. He L, Liu X, Zhao Z (2013) Non-isothermal kinetics study on synthesis of $LiFePO_4$ via carbothermal reduction method. Thermochim Acta 566:298–304
15. Jung J, Cho M, Zhou M (2013) Ab initio study of the fracture energy of $LiFePO_4$/$FePO_4$ interfaces. J Power Sources 243:706–714
16. Vediappan K, Guerfi A, Gariépy V et al (2014) Stirring effect in hydrothermal synthesis of nano C-$LiFePO_4$. J Power Sources 266:99–106
17. Ren Y, Bruce PG (2012) Mesoporous $LiFePO_4$ as a cathode material for rechargeable lithium ion batteries. Electrochem Commun 17:60–62
18. Lv Y-J, Long Y-F, Su J et al (2014) Synthesis of bowl-like mesoporous $LiFePO_4$/C composites as cathode materials for lithium ion batteries. Electrochim Acta 119:155–163
19. Wu Y-F, Liu Y-N, Guo S-W (2014) Hierarchical carbon-coated $LiFePO_4$ nano-grain microspheres with high electrochemical performance as cathode for lithium ion batteries. J Power Sources 256:336–344
20. Zhao Z, Si X, Liu X et al (2013) Li extraction from high Mg/Li ratio brine with $LiFePO_4$/$FePO_4$ as electrode materials. Hydrometallurgy 133:75–83
21. Gim J, Song J, Nguyen D et al (2014) A two-step solid state synthesis of $LiFePO_4$/C cathode with varying carbon contents for Li-ion batteries. Ceram Int 40:1561–1567
22. Tan L, Zhang L, Sun Q et al (2013) Capacity loss induced by lithium deposition at graphite anode for $LiFePO_4$/graphite cell cycling at different temperatures. Electrochim Acta 111:802–808
23. Zhang Y, Wu L, Zhao J et al (2014) A facile precursor-separated method to synthesize nano-crystalline $LiFePO_4$/C cathode materials. J Electroanal Chem 719:1–6
24. Xing Y, He Y-B, Li B, Chu X, Chen H, Ma J, Du H, Kang F (2013) $LiFePO_4$/C composite with 3D carbon conductive network for rechargeable lithium ion batteries. Electrochim Acta 109:512–518
25. Liu X, Chen X, Zhao Z, Liang X (2014) Effect of Na^+ on Li extraction from brine using $LiFePO_4$/$FePO_4$ electrodes. Hydrometallurgy 146:24–28
26. Liu S, Wang H (2014) WO_2 modified $LiFePO_4$/C cathode materials with improved electrochemical performance synthesized by in-situ synthesis method. Mater Lett 122:151–154
27. Mi CH, Cao GS, Zhao XP (2005) One-step solid-state synthesis and high-temperature electrochemical performance of carbon coated $LiFePO_4$ cathode. Chin J Inorg Chem 4:556–560
28. Kinomura N, Shimada M, Koizumi M et al (1976) Synthesis of a high pressure phase of $FePO_4$. Mater Res Bull 11(5):457–460
29. Ait-Salah A, Dodd J, Mauger A, Yazami R, Gendron F, Julien CM (2006) Structural and magnetic properties of $LiFePO_4$ and lithium extraction effects. Z Anorg Allg Chem 632:1598–1605
30. Scaccia S, Carewska M, Prosini PP (2004) Thermoanalytical study of iron(III) phosphate obtained by homogeneous precipitation from different media. Thermochim Acta 413:81–86
31. Laffont L, Delacourt C, Gibot P, Wu MY, Kooyman P et al (2006) Study of the $LiFePO_4$/$FePO_4$ two-phase system by high-resolution electron energy loss spectroscopy. Chem Mater 18:5520–5529
32. Delacourt C, Rodríguez-Carvajal J, Schmitt B, Tarascon JM, Masquelier C (2005) Crystal chemistry of the olivine-type Li_xFePO_4 system ($0 \le x \le 1$) between 25 and 370 °C. Solid State Sci 7:1506–1516
33. Meethong N, Huang HYS, Carter WC, Chiang YM (2007) Size-dependent lithium miscibility gap in nanoscale $Li_{1-x}FePO_4$. Electrochem Solid-State Lett 10:A134–A138
34. Aliounae N, Badeche T, Gagou Y et al (2000) Synthesis and phase transitions of iron phosphate. Ferroelectrics 241(1):255–262
35. Okadaa S, Yamamotoa T, Okazaki Y et al (2005) Cathode properties of amorphous and crystalline $FePO_4$. J Power Sources 146:570–574
36. Anderson AS, Thomas JO (2010) The source of first cycle capacity loss in $LiFePO_4$. J Power Sources 97–98:498–502
37. Chen G, Song X, Richardson TJ (2006) Electron microscopy study of the $LiFePO_4$ to $FePO_4$ phase transition. Electrochem Solid-State Lett 9:A295–A298
38. Ming T, Craig WC, Yet-Ming C (2010) Electrochemically driven phase transitions in insertion electrodes for lithium-ion batteries: examples in lithium metal phosphate olivines. Annu Rev Mater Res 40:501–529
39. Saiful IM, Daniel JD, Craig AJF et al (2005) Atomic-scale investigation of defects, dopants, and lithium transport in the $LiFePO_4$ olivine-type battery material. Chem Mater 17:5085–5092
40. Xu YB, Lu YJ, Yin P et al (2008) A versatile method for preparing $FePO_4$ and study on its electrode performance in lithium ion batteries. J Mater Process Technol 204:513–519
41. Qian LC, Xia Y, Zhang WK et al (2012) Electrochemical synthesis of mesoporous $FePO_4$ nanoparticles for fabricating high performance $LiFePO_4$/C cathode materials. Microporous Mesoporous Mater 152:128–133
42. Wang ZX, Wu L, Li XH et al (2008) Preparation of precursor and performance of $LiFePO_4$. J Funct Mater 4(39):614–617
43. Zhang MF, Hong JH, Yuan LJ et al (2009) Kinetics of dehydration of $FePO_4 \cdot 4H_2O$ in air. Chin J Inorg Chem 25(6):1022–1025
44. Boonchom B, Danvirutai C (2007) Thermal decomposition kinetics of $FePO_4 \cdot 3H_2O$ precursor to synthetize spherical nanoparticles $FePO_4$. Ind Eng Chem Res 46:9071–9076
45. Boonchom B, Puttawong S (2010) Thermodynamics and kinetics of the dehydration reaction of $FePO_4 \cdot 2H_2O$. Physica B 405:2350–2355
46. Okawa H, Yabuki J, Kawamura Y et al (2008) Synthesis of $FePO_4$ cathode material for lithium ion batteries by a sonochemical method. Mater Res Bull 43:1203–1208
47. Prosini PP, LiSi M, Scaccia S et al (2002) Synthesis and characterization of amorphous hydrated $FePO_4$ and its electrode performance in lithium batteries. J Electrochem Soc A149:297–300
48. Chang JY, Zhang JY, Feng T (2007) Preparation and performance test of $FePO_4$ precursor for high density $LiFePO_4$. J Yellow River Conservancy Tech Inst 23(3):51–54
49. Wang X, Yang XH, Zheng HG et al (2005) Synthesis and electrochemical performance of amorphous hydrated iron phosphate nanoparticles. J Cryst Growth 274:214–217
50. Song YN, Yang SF, Zavalij PY et al (2002) Temperature-dependent properties of $FePO_4$ cathode materials. Mater Res Bull 37:1249–1257
51. Hu GR, Zhou YL, Peng ZD et al (2007) Preparation and performance of $FePO_4$ precursor for $LiFePO_4$. Battery Bimonthly 37(5):339–341
52. Jiang DP, Zhang XJ, Lu SG et al (2011) Research on process of preparation and performance of iron phosphate as precusor of lithium iron phosphate. Rare Metals 30:52–54
53. Ma GC, Ting SW, Li Q et al (1993) Studies on synthesis and properties of iron(III) phosphate. J Hebei Univ (Sci Technol) 13(4):54–57
54. Xia JP, Deng XC, Wang LL (2010) Influence of synthesis time on the properties of $LiFePO_4$/C composites with self-produced $FePO_4$ as iron source. Chin Battery Ind 15(6):354–358
55. Lei M, Ying JR, Jiang CY et al (2006) Preparation and characteristic of high-density spherical $LiFePO_4$. Chin J Power Sources 30(1):11–13
56. Cao Y, Wang ZG, Yang H (2011) Synthesis and electrochemical properties of spherical $LiFePO_4$ with various particle sizes as cathode material for lithium ion batteries. J Funct Mater 3(42):448–451

57. Zhu YM, Tang SZ, Shi HH et al (2014) Synthesis of $FePO_4.xH_2O$ for fabricating submicrometer structured $LiFePO_4$/C by a co-precipitation method. Ceram Int 40:2685–2690
58. Gong FZ, Yi JH, Zhou LY et al (2009) Preparation of two kinds of $FePO_4$ powders with different morphologies and electrochemical properties of $LiFePO_4$. J Guangxi Univ Nat Sci Ed 34(6):731–735
59. Mal K, Bhaumik A, Matsukata M et al (2006) Syntheses of mesoporous hybrid iron oxophenyl phosphate, iron oxophosphate, and sulfonated oxophenyl phosphate. Ind Eng Chem Res 45:7748–7751
60. Guo XF (2000) Preparation, characterization and catalytic properties of nanoparticles and mesostructured materials. Nanjing University, Nanjing
61. Lu YJ, Xu YB, Yang RD et al (2007) A versatile method for preparing $FePO_4$ as a promising electrode material for rechargeable lithium batteries. J Lanzhou Univ (Nat Sci) 43(4):144–146
62. Zhu SM, Zhou HS, Hibino M et al (2004) Synthesis of hexagonal mesostructured $FePO_4$ using cationic surfactant as the template. Chem Lett 33(6):774–775
63. Shi ZC, Attia A, Ye WL et al (2008) Synthesis, characterization and electrochemical performance of mesoporous $FePO_4$ as cathode material for rechargeable lithium batteries. Electrochim Acta 53:2665–2673
64. Wang M, Xue YH, Zhang KL et al (2011) Synthesis of $FePO_4{\cdot}2H_2O$ nanoplates and their usage for fabricating superior high-rate performance $LiFePO_4$. Electrochim Acta 56:4294–4298
65. Zhou WJ, He W, Zhang XD et al (2009) Biosynthesis of iron phosphate nanopowders. Powder Technol 194:106–108
66. Cao F, Li DX (2010) Biotemplate synthesis of monodispersed iron phosphate hollow microspheres. Bioinspir Biomim 5:1748–3182
67. Chen YK, Okada S, Yamaki J-i (2002) Preparation of ferri phosphate and its application to lithium battery. J Huaqiao Univ (Nat Sci) 23(4): 407–411
68. Wu YL, Pu WH, Jiang CY et al (2012) Synthesis of nano $FePO_4$ and electrochemical characterization of composite cathode material $LiFePO_4$/C. J Inorg Mater 27(4):422–426
69. Delacourt C, Wurm C, Morcrette M et al (2003) Synthesis and thermal behavior of crystalline hydrated iron(III) phosphates of interest as positive electrodes in Li batteries. Chem Mater 15(26):5051–5058
70. Fan W (2009) Synthesis and electrochemical characterization of $FePO_4$ by a solid state reaction at low-heating temperature. Nanjing Normal University, Nanjing
71. Wang LN, Zhang ZG, Zhang KL (2007) A simple, cheap soft synthesis routine for $LiFePO_4$ using iron(III) raw material. J Power Sources 167:200–205